

The lifetime of binary black holes in Sérsic galaxy models

Nadia Biava,¹ Monica Colpi,^{1,2} Pedro R. Capelo,³ Matteo Bonetti,^{2,4}
Marta Volonteri,⁵ Tomas Tamfal,³ Lucio Mayer,³ and Alberto Sesana^{1,6}

¹*Department of Physics G. Occhialini, University of Milano-Bicocca, Piazza della Scienza 3, 20126 Milano, Italy*

²*National Institute of Nuclear Physics INFN, Milano-Bicocca, Piazza della Scienza 3, 20126 Milano, Italy*

³*Center for Theoretical Astrophysics and Cosmology, Institute for Computational Science, University of Zurich, Winterthurerstrasse 190, CH-8057 Zürich, Switzerland*

⁴*DiSAT, Università degli Studi dell'Insubria, Via Valleggio 11, 22100 Como, Italy*

⁵*Sorbonne Université, CNRS, UMR 7095, Institut d'Astrophysique de Paris, 98 bis bd Arago, 75014 Paris, France*

⁶*School of Physics and Astronomy and Institute of Gravitational Wave Astronomy, University of Birmingham, Edgbaston B15 2TT, UK*

15 March 2019

ABSTRACT

In the local universe, black holes of $10^{5-6} M_{\odot}$ are hosted in galaxies displaying a variety of stellar profiles and morphologies. These black holes are the anticipated targets of LISA, the Laser Interferometer Space Antenna that will detect the low-frequency gravitational-wave signal emitted by binary black holes in this mass interval. In this paper, we infer upper limits on the lifetime of binary black holes of $10^{5-6} M_{\odot}$ and up to $10^8 M_{\odot}$, forming in galaxy mergers, exploring two underlying stellar density profiles, by Dehnen and by Prugniel & Simien, and by exploiting local scaling relations between the mass of the black holes and several quantities of their hosts. We focus on the phase of the dynamical evolution when the binary is transitioning from the hardening phase ruled by the interaction with single stars to the phase driven by the emission of gravitational waves. We find that different stellar profiles predict very distinct trends with binary mass, with lifetimes ranging between fractions of a Gyr to more than 10 Gyr, and with a spread of about one order of magnitude, given by the uncertainties in the observed correlations, which are larger in the low-mass tail of the observed black hole population. Low-mass black hole binaries of $10^5 M_{\odot}$ develop larger eccentricities as they experience a longer-lasting interaction with the stellar background that help reduce their lifetimes during this phase.

Key words: black hole physics – gravitational waves – methods: numerical – galaxies: evolution – galaxies: kinematics and dynamics.

1 INTRODUCTION

The formation of a binary of two massive black holes in the aftermath of a galaxy-galaxy collision and its hardening down to the gravitational-wave (GW) domain is a challenging problem in stellar dynamics. Detailing the black hole dynamics from the large scale of a cosmological galactic merger (hundreds of kpc) to the tiny scale of GW inspiral (of the order of a few μpc) is instrumental in predicting the rate of black hole coalescences expected to occur during the hierarchical assembly of galaxies (Enoki et al. 2005; Rhoads & Wyithe 2005; Sesana et al. 2011a; Plowman et al. 2011; Klein et al. 2016; Tamanini et al. 2016; Bonetti et al. 2018a; Dayal et al. 2018; Ricarte & Natarajan 2018). The environment in which black hole pairing, binary formation, and contraction occur varies immensely. After years of studies, we learned that gas-free and gas-rich galaxy mergers show both

extremely complex and non-universal black hole dynamics (Colpi 2014; Mayer 2013).

There exist three main phases that black holes experience along the path to coalescence: (I) the early phase of pairing under dynamical friction in the stellar bulge of the post-merger galaxy, ending with the formation of a close Keplerian binary; (II) the phase of hardening by close encounters with single stars plunging on nearly radial orbits on to the binary or by viscous/gravitational angular momentum transport with gas in a circumbinary disc; and finally (III) the phase of GW inspiral.

With advances in numerical simulations, the duration of each phase is modulated by complex, interrelated processes. The inclusion of cosmology-driven initial conditions, cosmic gas inflows, rich galaxy morphology, asymmetries in the stellar distributions, gas dynamics, and a wider spectrum of galaxy and black hole mass ratios reveals the occurrence

of failures, bottlenecks, delays, rapid sinking, and/or erratic dynamics (Begelman et al. 1980; Milosavljević & Merritt 2003; Berczik et al. 2006; Mayer et al. 2007; Dotti et al. 2007; Callegari et al. 2008; Lodato et al. 2009; Callegari et al. 2011; Khan et al. 2011; Sesana et al. 2011b; Khan et al. 2012b,a, 2013; Fiacconi et al. 2013; Van Wassenhove et al. 2014; Vasiliev 2014; Vasiliev et al. 2015; Capelo et al. 2015; Roškar et al. 2015; del Valle et al. 2015; Lupi et al. 2015; Vasiliev 2016; Mayer et al. 2016; Khan et al. 2016; Goicovic et al. 2017; Capelo & Dotti 2017; Souza Lima et al. 2017; Pfister et al. 2017; Tamburello et al. 2017; Tremmel et al. 2017; Khan et al. 2018b; Bonetti et al. 2018b).

In this paper, we select a case that has not been studied at length, involving the hardening of *low-mass* supermassive black holes of mass $M_{\text{BH}} = 10^{5-8} M_{\odot}$ for which electromagnetic observations are less rich (for a recent review, see Mezcua 2017) than in the case of the giants of mass $10^{8-10} M_{\odot}$ and that are relevant for the Laser Interferometer Space Antenna (LISA), the low-frequency interferometer in space that will detect the GW emission from coalescing massive binary black holes in the low-mass tail (Amaro-Seoane et al. 2017; Barack et al. 2018).

As black hole coalescences of $10^{4-7} M_{\odot}$ can be detected with LISA from redshift $z \sim 0$ up to $z \sim 15-20$, when seed black holes form (Latif & Ferrara 2016), the environment in which they form and couple at dynamical level varies and evolves with redshift at the rhythm of the cosmic assembly of structures. High-resolution zoom-in simulations indicate that the stellar component, even in a gas-rich galaxy merger, is instrumental in driving the black holes to coalescence. A dense stellar cusp surrounding one or both black holes may form following a merger-driven, central gas inflow (Van Wassenhove et al. 2014; Khan et al. 2016), and it is in this dense environment that dynamical friction and later scattering of stars in a triaxial remnant guide the binary contraction.

Very recently, Tamfal et al. (2018) investigated the early phase of pairing of two black holes of $10^5 M_{\odot}$ in a merger between two dark-matter-dominated dwarf galaxies, using collisionless N -body simulations. They found that the efficiency of pairing, prior to binary formation and stellar hardening, depends sensibly on the steepness of the central dark matter density profile. Only cuspy dark matter profiles appear to be favourable to forming a Keplerian binary (of mean eccentricity $e \sim 0.5$), i.e. a bound state on sub-pc scales, when the mass in stars and dark matter inside the orbit decreases below the sum of the black hole masses. Due to the limited resolution (~ 1 pc) of these simulations, the dynamics of the black holes could not be reliably followed down to the stages in which close encounters with single stars and GW emission become important.

In this paper, we explore this next stage using analytical tools in order to guide future simulations on the dynamical evolution of black holes in dwarfs. We aim at determining the binary lifetime in its hardening phase over a mass range that extends from $10^8 M_{\odot}$ down to the least massive supermassive black holes of $10^5 M_{\odot}$. We investigate whether stalling of the binary in stellar systems (often referred to the “last-parsec problem”, discussed mostly in the context of supermassive black holes of $10^{8-9} M_{\odot}$) does occur also at the lower-mass end of the black hole mass distribution.

Direct N -body simulations of black hole hardening in

a triaxial stellar background indicate that a departure from spherical symmetry in the stellar nucleus of the galaxy (after the merger) keeps the rate of interaction of stars with the binary at a high enough level, even when the system is collisionless, so that the binary continues to shrink rather rapidly. A sufficiently high number of stars moving on centrophilic orbits appears to be present in non-spherical potentials to let the binary enter the GW driven phase (Merritt & Poon 2004; Holley-Bockelmann & Sigurdsson 2006). Using a Monte Carlo method, Vasiliev et al. (2015) confirmed this trend in triaxial galaxies without relaxation and showed that even a moderate departure from axisymmetry is sufficient to keep the binary shrinking (Vasiliev 2016). After performing a detailed comparison between direct N -body simulations and a hybrid model based on three-body scattering experiments (see, e.g. Quinlan 1996; Sesana et al. 2006), Sesana & Khan (2015) conjectured that the (N -body) binary hardening rate is equivalent to that of a binary embedded in a field of stars inside a spherical potential where key quantities such as the stellar density and velocity dispersion are evaluated at the binary gravitational sphere of influence. This enables to estimate the lifetime of the binary forming in a merger, based solely on a few key parameters of the host. Sesana & Khan (2015) confined their analysis to galaxies described by a Dehnen (1993) stellar profile and black holes with masses in excess of $10^7 M_{\odot}$, finding hardening time-scales ranging from a fraction of a Gyr to ~ 10 Gyr, with a strong dependence on the binary eccentricity. In light of recent findings that attribute to dwarf galaxies a variety of morphologies, the choice of the stellar density and velocity dispersion profile becomes then critical.

Reines et al. (2013; hereafter RGG) assembled the largest sample of local dwarf galaxies (with stellar masses in the interval $10^{8.5} < M_* < 10^{9.5} M_{\odot}$) hosting a nuclear black hole with median mass of $2 \times 10^5 M_{\odot}$, detected as a low-luminosity active galactic nucleus (see Mezcua et al. 2018 for a sample at high redshift). These galaxies display different morphologies, presence or absence of central pseudo-bulges, and different levels of compactness, with Sérsic (1963, 1968) indices varying from 0.8 to 6. As an example, the dwarf disc galaxy RGG 118 hosts the least massive black hole ever detected with mass $\sim 5 \times 10^4 M_{\odot}$. It contains a pseudo-bulge of $10^{8.5} M_{\odot}$, fit by an inner Sérsic profile of index $n = 0.8 \pm 0.1$, placing the black hole mass below the extrapolated value from the $M_{\text{BH}}-M_{\text{sph},*}$ relation defined by elliptical/S0 more massive galaxies (Baldassare et al. 2015, 2017), where $M_{\text{sph},*}$ is the total mass of the stellar spheroidal. The departure from the $M_{\text{BH}}-M_{\text{sph},*}$ relation is observed in a much wider sample of dwarf and spiral mega-maser galaxies (Kormendy & Ho 2013; Läscher et al. 2016; Reines & Volonteri 2015; Greene et al. 2008).

Savorgnan et al. (2013) have highlighted the occurrence of a correlation between the black hole mass and the Sérsic index of the host, showing that less massive black holes (below $10^7 M_{\odot}$ and of interest for LISA) live preferentially in galaxies with low values of $n < 2$. To anchor the black hole mass and, by extrapolation, the mass of the binary to the stellar profile of the underlying host, we here use the $M_{\text{BH}}-M_{\text{sph},*}$ correlation, and the looser relation $M_{\text{BH}}-n$, as inferred in Kormendy & Ho (2013), Scott et al. (2013), Savorgnan et al. (2013), and Davis et al. (2019). We recall that the Sérsic profile describes the surface brightness of a galaxy,

and the index n controls its degree of curvature, representing the generalization of the de Vaucouleurs' law ($n = 4$; de Vaucouleurs 1948, 1959). The smaller is the value of n , the shallower and less concentrated the profile. Most galaxies are fit by Sérsic profiles with indices in the range $1/2 < n < 10$ such that brighter, more massive galaxies tend to be fit with larger n .

In this paper, we provide an estimate of the black hole binary hardening times relevant for LISA considering either a Dehnen profile (for a comparison with the work of Sesana & Khan 2015) and a Prugniel & Simien (1997) profile, the latter relating the stellar distribution to the Sérsic surface brightness profile.

The paper is organized as follows. In Section 2, we model the transition between the hardening and GW emission as in Sesana & Khan (2015), in order to define the longest time of residence of a black hole binary in a given stellar background, which we refer to as binary lifetime. We then introduce the Dehnen (1993) and Prugniel & Simien (1997) models (Sections 2.1 and 2.2, respectively) and calculate characteristic time-scales and black hole binary separations for different values of the mass ratio and binary eccentricity, although in the rest of the paper we adopt circular binaries to focus on the stellar density at the binary black hole sphere of influence. We then consider the data sample of Graham & Scott (2015), and a study by Nguyen et al. (2018) to link these time-scales to the dormant black holes that we observe in the near universe. In Section 3, we show the strong dependence of our results on the choice of scaling relations, whereas a comparison between the two models is reported in Section 4. In Section 5, we derive our conclusions.

2 BINARY LIFETIME

Consider the case of a black hole binary embedded in a stellar spherical background. The binary hardens via scattering off single stars plunging on nearly radial orbits, and GW emission, which intervenes at the shortest distances. The evolution of the semi-major axis a is ruled by the two mechanisms and is given by the sum of two terms which have different scalings with a (Sesana & Khan 2015):

$$\frac{da}{dt} = \left. \frac{da}{dt} \right|_{3b} + \left. \frac{da}{dt} \right|_{gw} = -Aa^2 - \frac{B}{a^3}, \quad (1)$$

where the coefficients

$$A = \frac{GH\rho_{\text{inf}}}{\sigma_{\text{inf}}}, \quad B = \frac{64G^3qM_{\text{BH,T}}^3F(e)}{5c^5(1+q)^2} \quad (2)$$

describe the three-body 'star-black hole binary' close interaction and GW dissipation, respectively. The binary has total mass $M_{\text{BH,T}} = M_{\text{BH,1}} + M_{\text{BH,2}}$ and mass ratio $q = M_{\text{BH,2}}/M_{\text{BH,1}} \leq 1$. G is the gravitational constant and c is the speed of light in vacuum. The coefficient A depends on the ratio between the stellar density ρ_{inf} and velocity dispersion σ_{inf} at the black hole binary sphere of influence. Thus, information of the mass of the binary is implicitly contained in the values of the density and velocity dispersion of the underlying stellar system. H is a dimensionless hardening rate

inferred from three-body scattering experiments, of the order of ~ 15 – 20 (Quinlan 1996; Sesana et al. 2006), which we set equal to 15. The coefficient B , related to the GW energy loss, is a sensitive function of the binary eccentricity e , with the factor $F(e) = (1 - e^2)^{-7/2}[1 + (73/24)e^2 + (37/96)e^4]$ (Peters & Mathews 1963).

Since the stellar hardening rate is $\propto a^2$ and the GW hardening rate is $\propto a^{-3}$, binaries spend most of their time at the transition separation that can be estimated setting

$$|(da/dt)_{3b}| = |(da/dt)_{gw}|. \quad (3)$$

This occurs at a distance

$$a_{*/gw} = \left[\frac{64G^2\sigma_{\text{inf}}qM_{\text{BH,T}}^3F(e)}{5c^5(1+q)^2H\rho_{\text{inf}}} \right]^{1/5} \quad (4)$$

corresponding to a maximum in the hardening time-scale

$$t(a_{*/gw}) = \frac{\sigma_{\text{inf}}}{GH\rho_{\text{inf}}a_{*/gw}}, \quad (5)$$

which we refer to as binary lifetime in the following. $t(a_{*/gw})$ displays a weak dependence on the mass ratio q , scaling as $q^{1/5}$, and a stronger dependence on the eccentricity, scaling as $t(a_{*/gw}) \propto (1 - e^2)^{7/10}$ (e.g. a reduction of a factor of 3.2 can be attained when the eccentricity is 0.9 compared to $e = 0$).

Scattering experiments and direct N -body numerical simulations (e.g. Sesana et al. 2011b; Khan et al. 2012b, 2018a,b) indicate that the binary eccentricity increases during the hardening phase by three-body scatterings. Thus, we couple Equation (1) with the evolution equation for e , which accounts for the effects of stellar scatterings and GW circularisation,

$$\frac{de}{dt} = a \frac{G\rho_{\text{inf}}HK}{\sigma_{\text{inf}}} - \frac{304}{15} \frac{G^3qM_{\text{BH,T}}^3}{c^5(1+q)^2a^4(1-e^2)^{5/2}} \left(e + \frac{121}{304}e^3 \right), \quad (6)$$

where the eccentricity growth rate K is a numerical factor, calibrated against scattering experiments, which depends on e and is of order ~ 0 (for low values of e) and ~ 0.2 otherwise (Quinlan 1996; Sesana et al. 2006).

Before proceeding, we need to estimate σ_{inf} and ρ_{inf} . We do this for two different physical models.

2.1 Dehnen density profile

Sesana & Khan (2015) calculated the coalescence time of a binary using as a reference model for the galaxy remnant the density profile described by Dehnen (1993):

$$\rho(r) = \frac{(3-\gamma)M_{\text{sph,*}}}{4\pi} \frac{r_0}{r^\gamma(r+r_0)^{(4-\gamma)}}, \quad (7)$$

where r_0 is the scale radius and $0 \leq \gamma < 3$ the inner logarithmic slope. The velocity dispersion profile associated to this model is

$$\sigma^2(r) = GM_{\text{sph,*}}r^\gamma(r+r_0)^{4-\gamma} \int_r^\infty dr' \frac{r'^{(1-2\gamma)}}{(r'+r_0)^{(7-2\gamma)}}. \quad (8)$$

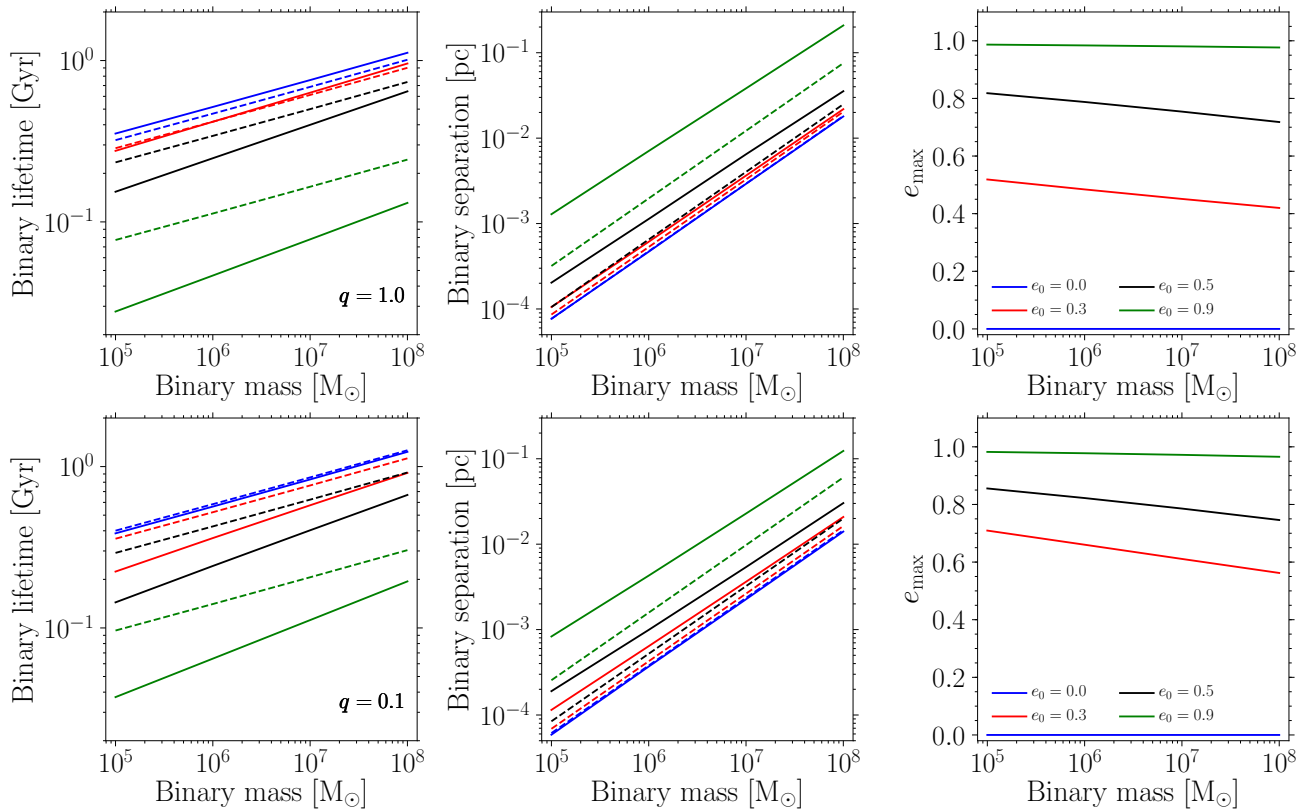


Figure 1. Lifetime $t(a_{*/\text{gw}})$ (left-hand panels), characteristic separation $a_{*/\text{gw}}$ (central panels), and maximum eccentricity reached e_{max} (right-hand panels) as a function of the binary total mass, considering four different initial eccentricities ($e_0 = 0.0, 0.3, 0.5$, and 0.9), for a mass ratio $q = 1$ (top panels) and 0.1 (bottom panels). We remark that the mean eccentricity of the Keplerian binary at the end of the cuspy simulation in [Tamfal et al. \(2018\)](#) is ~ 0.5 . The density and velocity dispersion of the underlying host are computed using the Dehnen profile with index $\gamma = 1$. In the left-hand and central panels, solid and dashed lines show the evolution of the binary’s lifetime and characteristic separation when considering an evolving and fixed eccentricity, respectively. From the right-hand panel, it is evident that, at lower masses, binaries can acquire a higher eccentricity as a consequence of the longer interaction with the stellar background (except when $e_0 = 0.0$, for which $K \sim 0$). We note that $t(a_{*/\text{gw}}) \propto q^{1/5}$.

The Dehnen profile (see also [Tremaine et al. 1994](#)) is an analytical model which is a generalisation of widely used models such as the [Hernquist \(1990; \$\gamma = 1\$ \)](#) and [Jaffe \(1983; \$\gamma = 2\$ \)](#) profiles. In projection, for $\gamma \sim 3/2$, it resembles quite well the de Vaucouleurs’ law $R^{1/4}$ profile ([de Vaucouleurs 1948, 1959](#)), which describes how the surface brightness of ellipticals and bulges of spirals varies as a function of the projected distance R from the centre.

To evaluate the density and velocity dispersion at the black hole binary sphere of influence $r = r_{\text{inf}}$, we need to correlate the black hole binary mass with the stellar mass. Under the assumption that scaling relations can be applied to the binary, when the merger is near completion, we proceed as follows:

- The stellar (bulge) mass $M_{\text{sph},*}$ is inferred from the $M_{\text{BH}}-M_{\text{sph},*}$ relation taken from [Kormendy & Ho \(2013\)](#): $M_{\text{BH},\text{T}}/10^9 M_{\odot} = 0.49(M_{\text{sph},*}/10^{11} M_{\odot})^{1.16}$.
- The effective radius R_{eff} is a function of the galaxy stellar mass and depends on the nature of the galaxy host. For massive ellipticals, bulges of spirals, and ultra-compact dwarfs, [Dabringhausen et al. \(2008\)](#) found $R_{\text{eff}}/\text{pc} = 2.95(M_{\text{sph},*}/10^6 M_{\odot})^{0.596}$.
- The scale radius r_0 is connected to the bulge effective

radius R_{eff} through the relation $R_{\text{eff}} \sim 0.75r_0(2^{1/(3-\gamma)} - 1)^{-1}$ ([Dehnen 1993](#)).

- The influence radius, defined as the radius containing twice the binary mass in stars, i.e. $M_*(< r_{\text{inf}}) = 2M_{\text{BH},\text{T}}$, is given by $r_{\text{inf}} = r_0 / \{ [M_{\text{sph},*} / (2M_{\text{BH},\text{T}})]^{1/(3-\gamma)} - 1 \}$.
- The stellar density ρ_{inf} is obtained from Equation (7) at the influence radius.
- The velocity dispersion σ_{inf} is computed using Equation (8).¹

With the above prescriptions, we relate in a unique way $M_{\text{BH},\text{T}}$ to the properties of the host galaxy: $M_{\text{sph},*}$, r_0 , R_{eff} , r_{inf} , ρ_{inf} , and σ_{inf} . This enables us to solve Equations (1) and (6), for different values of the initial eccentricity e_0 and an initial binary separation equal to the radius a_0 at which the enclosed stellar mass is equal to $2M_{\text{BH},\text{T}}$ (when a Keplerian binary forms). We then compute the characteristic separation $a_{*/\text{gw}}$ and the corresponding lifetime $t(a_{*/\text{gw}})$ as a function of the binary mass, from Equations (4) and (5), for a given value of γ , q , and e_0 . This

¹ In [Sesana & Khan \(2015\)](#), σ_{inf} was computed using the $M_{\text{BH}}-\sigma$ correlation by [Kormendy & Ho \(2013\)](#). We note, however, that this choice does not significantly change the results.

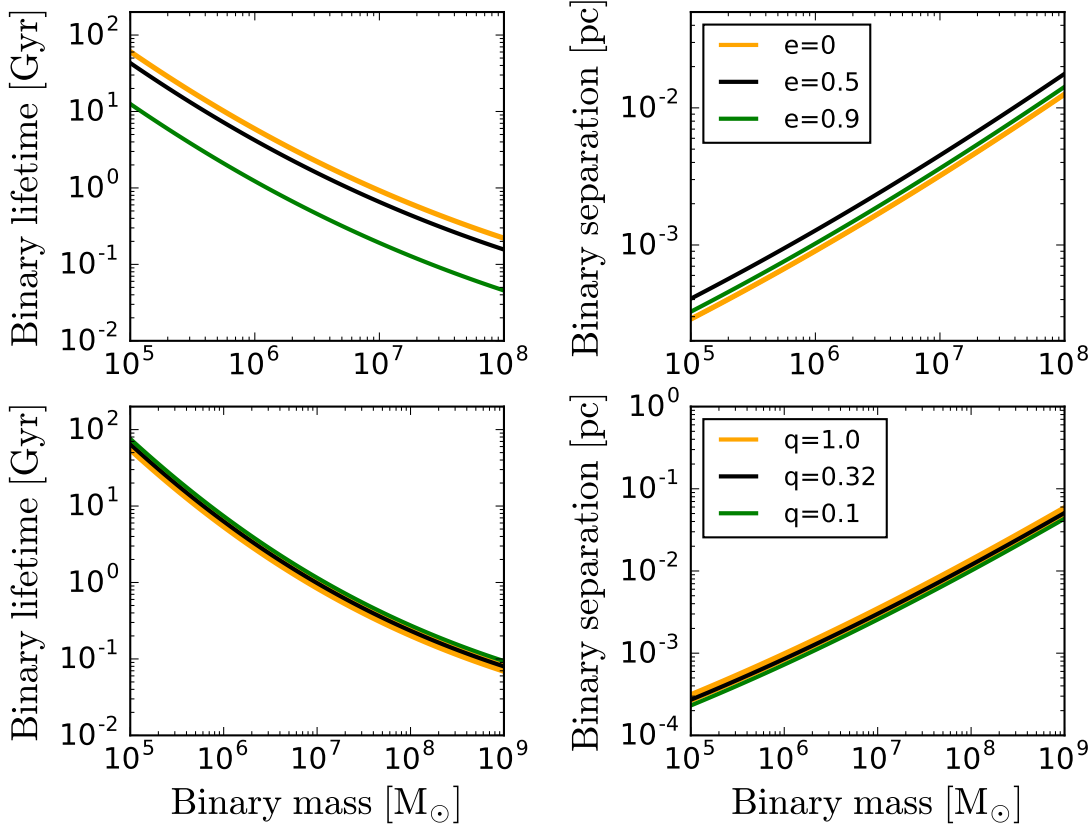


Figure 2. Lifetime (left-hand panels) and characteristic separation (right-hand panels) of massive black hole binaries versus binary mass, assuming the ‘black hole mass–Sérsic index n ’ relation given by Equation (12) for galaxies described by the Prugniel & Simien profile, for (upper panels) equal mass ($q = 1$) binaries with constant, unevolved eccentricity $e = 0, 0.5$, and 0.9 (orange, black, and green, respectively) and for (bottom panels) constant unevolved eccentricity $e = 0$ with different mass ratio $q = 1.0, 0.32$, and 0.1 (orange, black, and green, respectively). For the influence radius, we use here an average value of $r_{\text{inf}} = 0.023R_{\text{eff}}$, deduced fitting the data of [Graham & Scott \(2015\)](#).

is illustrated in Figure 1, where we fix $\gamma = 1$ and consider two values of the mass ratio $q = 0.1$ and 1 (we do not consider lower values of the mass ratio, as minor mergers with $q \lesssim 0.1$ may lead to wandering black holes; [Callegari et al. 2008, 2011; Colpi 2014](#)). In Figure 1, e_{max} is the maximum binary eccentricity attained during evolution.

We note that lifetimes cover a wide range, from 30 Myr up to 1 Gyr, show very weak dependence on q , and depend sensitively on e_0 . LISA black hole binaries need to attain tiny separations compared to galactic scales, of the order of 10^{-3} pc ($e_0 = 0.9$) and 10^{-4} pc ($e_0 = 0.3$) for the lightest binaries of $10^5 M_{\odot}$. These relations, computed using the expression of the velocity dispersion at the gravitational sphere of influence of the binary, are close to the ones computed by [Sesana & Khan \(2015\)](#), who assumed non-evolving values of the eccentricity at the transition between stellar hardening and GW emission. We note that accounting for the eccentricity evolution reduces the binary lifetime by a factor of ~ 2 – 10 . Thus, in the following analysis, we treat the eccentricity as a constant and equal to zero, so that time-scales provide an upper limit. Note that, if the relevant radius at which the loss cone is kept full is $r_{\text{inf}} = GM_{\text{BH,T}}/\sigma^2(r_{\text{inf}})$, then the time-scales decrease by a factor of ~ 2 .

2.2 Prugniel and Simien density profile

Galaxies in the [Graham & Scott \(2015\)](#) data set are divided in Sérsic and core-Sérsic galaxies. The term *Sérsic galaxy* is used to denote galaxies (ellipticals and bulges of disc galaxies) whose surface brightness I is described by the Sérsic model ([Sérsic 1963, 1968](#)), $I \propto R^{1/n}$. The term *Core-Sérsic galaxy* refers to a galaxy whose main spheroidal component has a partially depleted core (i.e. a central stellar deficit of light that is not due to dust, enclosed in a radius $R \sim 0.01R_{\text{eff}}$) such that the surface brightness profile is well described by the core-Sérsic model ([Graham et al. 2003](#)), which joins a single inner power-law profile to an outer Sérsic profile. [Scott et al. \(2013\)](#) have found that the $M_{\text{BH}}-M_{\text{sph,*}}$ relation is different for this type of galaxies: core-Sérsic galaxies follow a linear relation, whereas Sérsic galaxies a quadratic one. The bend in the relation occurs at $M_{\text{BH}} \sim 2 \times 10^8 M_{\odot}$, with Sérsic galaxies hosting the smallest black holes.

We calculate again the binary lifetime considering only Sérsic galaxies, which host central black holes in the range of interest of LISA. This time, however, we use the density profile developed by [Prugniel & Simien \(1997\)](#) to describe Sérsic galaxies (a complete analysis of the model is reported

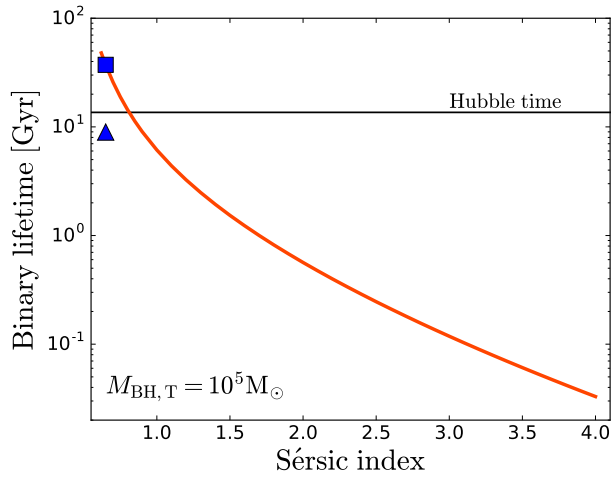


Figure 3. Binary lifetime versus Sérsic index n , for a black hole binary of $10^5 M_{\odot}$. The blue square indicates the time evaluated in this work binding the effective radius to the stellar mass of the galaxy with the relation found by [Dabringhausen et al. \(2008\)](#) and estimating the Sérsic index from the [Savorgnan et al. \(2013\)](#) relation, using a constant eccentricity of $e = 0$. The blue triangle indicates the time derived assuming $e = 0.9$ (this value is close to e_{\max} given in Figure 1 for a binary of $10^5 M_{\odot}$, when starting from $e_0 = 0.5$, the mean eccentricity at the end of the cuspy simulation in [Tamfal et al. 2018](#)). The horizontal line indicates the Hubble time.

in [Terzić & Graham 2005](#)). Density as a function of radius r is given by

$$\rho(r) = \rho_0 \left(\frac{r}{R_{\text{eff}}} \right)^{-p} e^{-b(r/R_{\text{eff}})^{1/n}}, \quad (9)$$

which depends on the curvature of the profile n , the normalization factor ρ_0 , and the effective radius R_{eff} . The parameters p and b are a function of n , as described below. The velocity dispersion is given by

$$\sigma^2(r) = \frac{4\pi G \rho_0^2 R_{\text{eff}}^2 n^2 b^{2n(p-1)}}{\rho(r)} \int_Z^{\infty} \bar{Z}^{-n(p+1)-1} e^{-\bar{Z}} \gamma[n(3-p), \bar{Z}] d\bar{Z} \quad (10)$$

where $Z = b(r/R_{\text{eff}})^{1/n}$, and here γ is the lower incomplete Gamma function.

The parameters used in these equations are calculated from the following relations:

- The stellar mass of the spheroid is inferred either from ([Scott et al. 2013](#))

$$M_{\text{BH,T}}/10^7 M_{\odot} = 7.89 (M_{\text{sph,*}}/2 \times 10^{10} M_{\odot})^{2.22}, \quad (11)$$

when evaluating the trends of Figure 2, or directly from the sample of [Graham & Scott \(2015\)](#), when plotting the data-points of Figure 4.

- R_{eff} is connected to the stellar mass through the relation $R_{\text{eff}}/\text{pc} = 2.95 (M_{\text{sph,*}}/10^6 M_{\odot})^{0.596}$ for the bulges of spirals and ultra-compact dwarfs ([Dabringhausen et al. 2008](#)).

- The index n is connected to the black hole mass through

the relation taken from [Savorgnan et al. \(2013\)](#) for Sérsic bulges:

$$\log_{10}(M_{\text{BH,T}}/M_{\odot}) = 7.73 + 4.11 \log_{10}(n/3). \quad (12)$$

- p is connected to n by $p = 1.0 - 0.6097/n + 0.05563/n^2$, for $0.6 < n < 10$ and $10^{-2} \leq r/R_{\text{eff}} \leq 10^3$ ([Márquez et al. 2000](#)). This relation is obtained through a high-quality match between the exact, de-projected Sérsic profiles (solved numerically) and the above expression of $\rho(r)$.

- b is chosen to ensure that R_{eff} contains half the (projected) galaxy light and is obtained by solving the equation $\Gamma(2n) = 2\gamma(2n, b)$, where Γ and γ are the Gamma and lower incomplete Gamma function, respectively. A good approximation of b for $0.5 < n < 10$ is $b = 2n - 1/3 + 0.009876/n$ ([Prugniel & Simien 1997](#)).

- The density ρ_0 is inferred from Equation (9) through integration over the mass distribution.

- The binary influence radius r_{inf} has been deduced for every galaxy in the sample from the relation $r_{\text{inf}} = GM_{\text{BH,T}}/\sigma^2(r_{\text{inf}})$.

In Figure 2, we plot the binary lifetime and separation as a function of $M_{\text{BH,T}}$ for different values of (unevolved) eccentricity and mass ratio. In Sérsic galaxy models, the binary lifetime increases with decreasing binary mass, in contrast to the Dehnen model (Figure 1). This trend mirrors the correlation between the black hole mass and the index n , as lower-mass black holes are hosted in galaxies with lower values of n . The binary lifetime is proportional to $(\sigma_{\text{inf}}/\rho_{\text{inf}})^{4/5}$ [see Equations (4) and (5)] which, in Prugniel & Simien models with low n , increases with decreasing n . We find that the transition separation $a_{*/\text{gw}}$ falls in a similar way to that of the Dehnen models.

Figure 3 shows the lifetime of a binary black hole of $10^5 M_{\odot}$ in a host galaxy of $1.3 \times 10^9 M_{\odot}$ as a function of the Sérsic index n , to illustrate the dependence of this time-scale on this index, which determines both the density and dispersion velocity at the binary black hole influence radius.

3 LIFETIMES: BLACK HOLE MASS VERSUS SÉRSIC INDEX

In this section, we show the strong dependence of the binary lifetimes on the Sérsic index. In Figure 4, we plot with orange dots the binary lifetime calculated for the black holes in the [Graham & Scott \(2015\)](#) sample (for the case $q = 1, e = 0$) using Equation (12). Lifetimes range between 0.3 Gyr and the Hubble time for black hole binaries with masses above a few $10^5 M_{\odot}$, but exceed the Hubble time for lighter binaries. These lifetimes are upper limits, as binaries are expected to develop large eccentricities during the hardening which reduce the value by factors of ~ 2 – 5 (see Figure 2).

Recently, [Davis et al. \(2019\)](#) proposed a revised version of the $M_{\text{BH}}-n$ relation:

$$\log_{10}(M_{\text{BH,T}}/M_{\odot}) = 7.45 + 2.76 \log_{10}(n/2.20). \quad (13)$$

This new relation gives lower values of n for a given (low) black hole mass, compared to the relation by [Savorgnan et al. \(2013\)](#). Red dots in Figure 4 indicate binary lifetimes inferred using Equation (13), for a few select black holes.

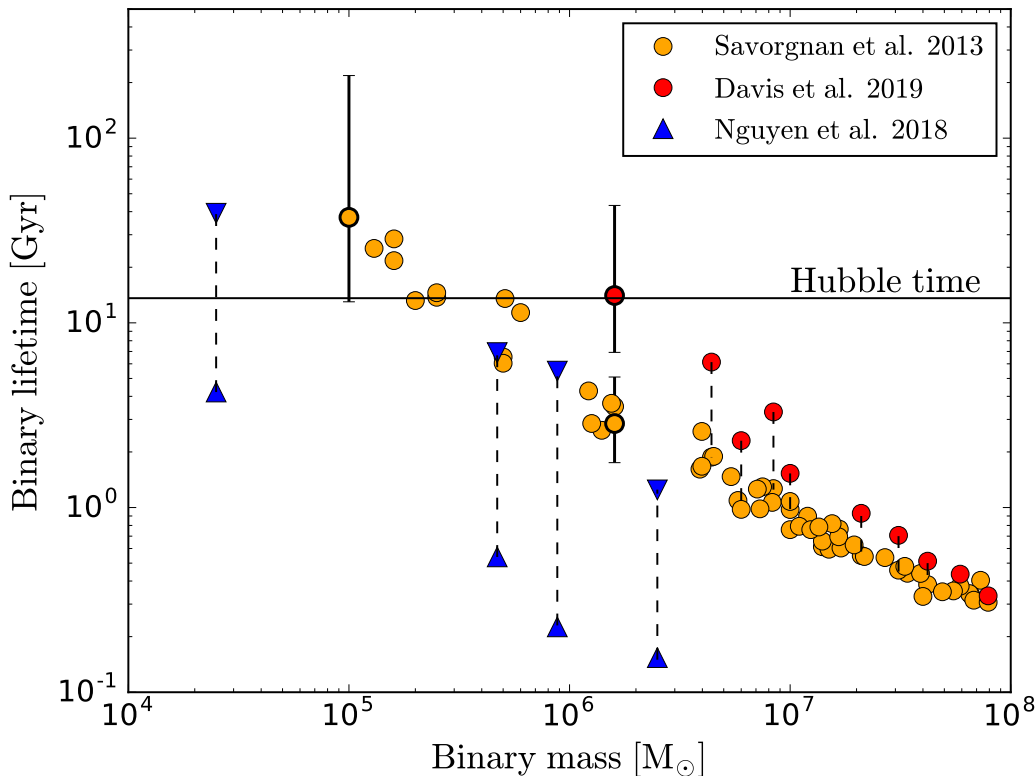


Figure 4. Binary lifetime versus binary mass for the samples of Sérsic galaxies taken from [Graham & Scott \(2015\)](#) (orange dots) and [Nguyen et al. \(2018\)](#) (upper blue triangles), using the Prugniel & Simien stellar density profile, and correlating the binary mass with the Sérsic index n , using Equation (12) from [Savorgnan et al. \(2013\)](#). We also show the lifetimes computed directly from the data given in [Nguyen et al. \(2018\)](#) (lower blue triangles). The red dots show the binary lifetimes computed for select galaxies of the same sample of [Graham & Scott](#) but now inferred using Equation (13) from [Davis et al. \(2019\)](#). For two values of the binary mass of $10^5 M_\odot$ and $1.6 \times 10^6 M_\odot$, we also show the error associated to the uncertainties of the relations described by Equations (12) (for both values of the masses) and (13) (for $1.6 \times 10^6 M_\odot$ only). The binary has mass ratio $q = 1$ and eccentricity $e = 0$, kept constant. Thus, the plot provides upper limits to the binary lifetime. The Hubble time is indicated by a horizontal line.

Both relations have a very large scatter, and we computed the uncertainty on $t(a_{*,\text{gw}})$ for two select black hole mass (10^5 and $1.6 \times 10^6 M_\odot$) highlighted in Figure 4 with black circles and associated errors. For example, using the Davis et al. (Savorgnan et al.) relation and scatter, the uncertainty on $t(a_{*,\text{gw}})$ when $M_{\text{BH,T}} = 1.6 \times 10^6 M_\odot$ is of a factor of 7–8 (of 2). For $M_{\text{BH,T}} = 10^5 M_\odot$, the scatter is ~ 10 using Savorgnan et al.

[Nguyen et al. \(2018\)](#) published a high-resolution study of four black holes hosted in nearby low-mass early-type galactic nuclei (M32, NGC 205, NGC 5102, and NGC 5206), providing the values of the black hole mass, host galaxy stellar mass, bulge Sérsic index, bulge effective radius, and black hole influence radius, for each of these galaxies. We computed the expected binary lifetimes using the published values of M_{BH} , n , R_{eff} , r_{inf} and the Prugniel & Simien model for the density and stellar dispersion at r_{inf} (lower blue triangles in Figure 4), and compared them with the ones we inferred using Equation (12) (upper blue triangles). In Figure 4, we show how the binary lifetime decreases by one order of magnitude when using the data from [Nguyen et al. \(2018\)](#) instead of the relations in Section 2.2.

This illustrates how sensitive is the dependence of the

binary lifetimes on the underlying properties of the stellar background.

4 DEHNEN VERSUS PRUGNIEL & SIMIEN

It is interesting to carry out a direct comparison between the two models. To this purpose, we calculate the binary lifetime for the galaxies of the [Graham & Scott \(2015\)](#) sample, using both the Dehnen profile (varying γ), and the Prugniel & Simien model along the $M_{\text{BH}}-n$ correlation of Equation (12). For consistency, we define the binary influence radius as $r_{\text{inf}} = GM_{\text{BH,T}}/\sigma^2(r_{\text{inf}})$ for both models. Figure 5 gives in black, blue, and red the time-scales corresponding to the Dehnen slopes $\gamma = 0.5, 1.0$, and 1.5 , respectively. In orange, we give the result of the Prugniel & Simien model to contrast the different trends of $t(a_{*/\text{gw}})$ with the black hole binary mass.

This difference can be understood by comparing, amongst the different models, the values of the density and velocity dispersion at the binary gravitational influence radius as highlighted in Figure 6. The dependence of both density and velocity dispersion on $M_{\text{BH,T}}$ comes from the correlations $M_{\text{BH}}-M_{\text{sph},*}$, $M_{\text{BH}}-n$, and $R_{\text{eff}}-M_{\text{sph},*}$, and from

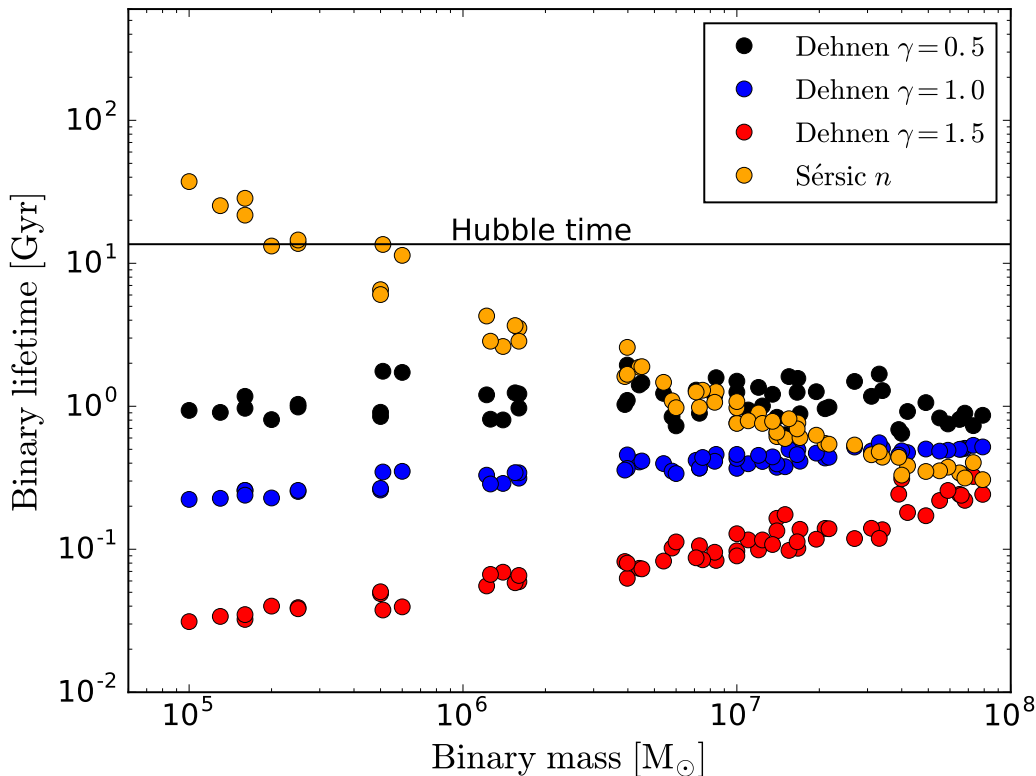


Figure 5. Binary lifetimes versus binary mass for the sample of Sérsic galaxies taken from [Graham & Scott \(2015\)](#), using the Prugniel & Simien stellar density profile in orange as in Figure 4. For a comparison, black, blue, and red dots refer to the same data-set but computing the binary lifetime $t_{*/\text{gw}}$ using Dehnen profiles with $\gamma = 0.5, 1.0,$ and $1.5,$ respectively. For homogeneity in the comparison, we computed here the black holes sphere of influence in terms of the stellar velocity dispersion. The Hubble time is indicated by a horizontal line.

r_{inf} itself. We note a remarkable difference among the values of the densities $\rho(r_{\text{inf}})$ between the Dehnen and the Prugniel & Simien models. In all Dehnen profiles, the stellar density is a decreasing function of the black hole binary mass and can reach values as high as $\sim 10^5 \text{ M}_{\odot} \text{ pc}^{-3}$ for $M_{\text{BH,T}} = 10^5 \text{ M}_{\odot}$ and $\gamma = 1.5$. Moreover, the change in stellar density is more pronounced for higher values of γ . By contrast, in Sérsic galaxies, the run of $\rho(r_{\text{inf}})$ versus $M_{\text{BH,T}}$ is the opposite, with remarkably lower values, down to about $\sim 100 \text{ M}_{\odot} \text{ pc}^{-3}$ for $M_{\text{BH,T}} = 10^5 \text{ M}_{\odot}$. The density changes by a factor of ~ 10 over the entire range of black hole binary masses. There is no noticeable difference instead in the values of the stellar velocity dispersion between the two families of models.

5 CONCLUSIONS

In this paper, we carried on an estimate of the hardening time of black hole binaries in the mass interval between 10^5 and 10^8 M_{\odot} , relevant for LISA ([Amaro-Seoane et al. 2017](#)), under the assumption that binary contraction is driven by individual scatterings off stars. To this aim, we employed the empirical relation for the binary lifetime described in [Sesana & Khan \(2015\)](#), assuming that the black holes inhabit the stellar, central environment of local galaxies. In the analysis, we used two different models for the underlying stellar density and velocity dispersion profiles: the [Dehnen \(1993\)](#)

model and the [Prugniel & Simien \(1997\)](#) model, the latter describing galaxies with surface brightness fit by the Sérsic profile. Using local observed correlations between the black hole mass M_{BH} and the mass of the spheroid $M_{\text{sph,*}}$ ([Kormendy & Ho 2013](#); [Scott et al. 2013](#)), and the Sérsic index n ([Savorgnan et al. 2013](#); [Davis et al. 2019](#)) of the underlying host galaxy, we find different trends and a large spread of the binary lifetimes.

In Sérsic galaxies, described by a Prugniel & Simien profile, binary lifetimes increase with decreasing mass and exceed the Hubble time below $\sim 5 \times 10^5 \text{ M}_{\odot}$. These time-scales have been computed assuming null eccentricity, thus providing upper limits. In high-resolution simulations of isolated collisions between dwarf galaxies, [Tamfal et al. \(2018\)](#) find that, when a binary forms, it already carries a rather large eccentricity, with mean $e \sim 0.5$. Furthermore, we know that binaries increase their eccentricity during the hardening phase by stellar scattering. Thus, when considering the eccentricity evolution, lifetimes are comparable to/smaller than the Hubble time. We further caution that uncertainties in the observed correlations (which are larger in the low-mass tail of the observed black hole population) give a spread of about one order of magnitude.

If Dehnen profiles represent the underlying stellar population of galaxies hosting black holes, we find that binary lifetimes display a nearly constant or decreasing trend with decreasing black hole binary mass. Depending on the slope of

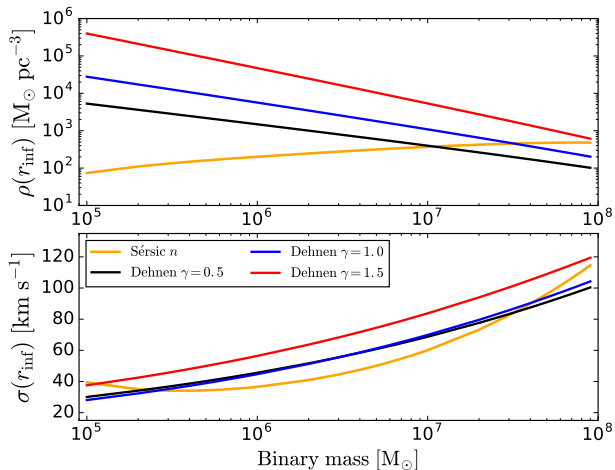


Figure 6. Upper panel: stellar density evaluated at the binary gravitational influence radius, $\rho(r_{\text{inf}})$, versus binary mass. Bottom panel: same for the stellar velocity dispersion, $\sigma(r_{\text{inf}})$. The orange lines refer to the Prugniel & Simien profile, along the $M_{\text{BH}}-n$ correlation [Equation (12)], whereas the red, blue, and black lines refer to the Dehnen profile with $\gamma = 1.5, 1.0$, and 0.5 , respectively.

the Dehnen profile, lifetimes are overall in the range between 30 Myr and 2 Gyr. If Dehnen profiles and high Sérsic indices are representative only of the high-mass tail ($\gtrsim 10^7 M_{\odot}$) of the black hole population, the black holes for which LISA will be most sensitive are subject to time delays that can span a wide range, depending on how steeply the stellar profiles rise within their gravitational sphere of influence.

Recent high-resolution observations of four strongly nucleated dwarf elliptical galaxies which host a central black hole (Nguyen et al. 2018) provided Sérsic indices systematically larger ($n > 1.4$ for the bulge component) than those expected from the correlations by Savorgnan et al. (2013) and Davis et al. (2019), yielding lifetimes even lower than 1 Gyr. Such galaxies are not rare, as about 25 per cent of galaxies in the field and in clusters are nucleated (Baldassare et al. 2014). Broadly speaking, low-mass galaxies show a range of profiles with inner logarithmic density slopes ranging from 0 to -4 (Gebhardt et al. 1996; Glass et al. 2011; Geha et al. 2017; Muñoz et al. 2018), with a tendency to have steeper profiles out to magnitudes of at least about -16 (Gebhardt et al. 1996), corresponding to stellar masses of about $5 \times 10^8 M_{\odot}$ and, presumably, to black holes with masses in the range 10^5 – $10^6 M_{\odot}$, whereas very faint dwarfs such as dwarf spheroidals have shallow profiles and light deficit. Only a small fraction of dwarf spheroidals or galaxies of similar mass are however expected to host central black holes (Van Wassenhove et al. 2010). For black holes hosted in galaxies with cored profiles and dark matter-dominated, such as dwarf spheroidals, a bottleneck exists along the path to coalescence in the early stages of the merger, ruled by dynamical friction (Read et al. 2006). The drag exerted on the black hole mainly by the dark matter background is not effective enough and this leads to a failure (or major delay) in the formation of a binary, which is the phase anticipating that of stellar hardening (Tamfal et al. 2018). Thus, LISA coalescence events with binary black holes of a few $10^5 M_{\odot}$ require dense environments.

We remind the reader that our results rely on obser-

vations (e.g. scaling relations) of the local universe. Thus, our estimates of the lifetimes depict hypothetical mergers at $z \lesssim 1$. At higher redshifts ($1 \lesssim z \lesssim 3$), galaxies show evolution in their averaged size (at fixed stellar galaxy mass) with R_{eff} scaling as $(1+z)^{-\alpha}$, with α varying from 0.7 (for late-type galaxies) to 1.48 (for early-type galaxies) (van der Wel et al. 2014). Thus, at $z \sim 3$, a factor of ~ 4 in the reduction of the effective radius can lead to an increase of ~ 64 in the density, if the galaxy model can be scaled self-similarly. Indeed, one recent study on massive galaxy mergers (Khan et al. 2016) showed the hardening time of two massive black holes to decrease from $\gtrsim 10$ Gyr at $z = 0$ to $\sim 10^7$ yr at $z = 3.3$ (see also the discussion in Mayer 2017). We expect the trend to be in the same direction, and there is the need to enlarge the sample of high-resolution simulations to consolidate this argument. However, one should remain aware that also simulations have uncertainties and results, especially for very local quantities, are dependent on sub-grid physics and resolution.

Mergers of LISA black holes at very high redshift ($z \sim 10$) are even more difficult to model, as cosmological simulations are hampered by lack of resolution on the low-mass scales involved in this process (Tremmel et al. 2017). The black hole dynamics is by far more complex to describe, as halos are non-relaxed systems and subjected to repeated, multiple interactions. Gas clumps can make the dynamics stochastic, and star formation and feedback can change the underlying background, broadening significantly the lifetime distribution for the binaries in the LISA-relevant mass range (Bellovary et al. 2019; Pfister et al. 2019). Delay times between halo-halo mergers and black hole mergers can be computed using semi-analytical models which include also the formation of triple systems as a vehicle for the formation and coalescence of these light black holes (Bonetti et al. 2018a).

REFERENCES

- Amaro-Seoane P., et al., 2017, preprint, ([arXiv:1702.00786](https://arxiv.org/abs/1702.00786))
- Baldassare V. F., Gallo E., Miller B. P., Plotkin R. M., Treu T., Valluri M., Woo J.-H., 2014, *ApJ*, **791**, 133
- Baldassare V. F., Reines A. E., Gallo E., Greene J. E., 2015, *ApJ*, **809**, L14
- Baldassare V. F., Reines A. E., Gallo E., Greene J. E., 2017, *ApJ*, **850**, 196
- Barack L., et al., 2018, preprint, ([arXiv:1806.05195](https://arxiv.org/abs/1806.05195))
- Begelman M. C., Blandford R. D., Rees M. J., 1980, *Nature*, **287**, 307
- Bellovary J. M., Cleary C. E., Munshi F., Tremmel M., Christensen C. R., Brooks A., Quinn T. R., 2019, *MNRAS*, **482**, 2913
- Berczik P., Merritt D., Spurzem R., Bischof H.-P., 2006, *ApJ*, **642**, L21
- Bonetti M., Sesana A., Haardt F., Barausse E., Colpi M., 2018a, preprint, ([arXiv:1812.01011](https://arxiv.org/abs/1812.01011))
- Bonetti M., Haardt F., Sesana A., Barausse E., 2018b, *MNRAS*, **477**, 3910
- Callegari S., Mayer L., Kazantzidis S., 2008, *Mem. Soc. Astron. Italiana*, **79**, 1302
- Callegari S., Kazantzidis S., Mayer L., Colpi M., Bellovary J. M., Quinn T., Wadsley J., 2011, *ApJ*, **729**, 85
- Capelo P. R., Dotti M., 2017, *MNRAS*, **465**, 2643

- Capelo P. R., Volonteri M., Dotti M., Bellovary J. M., Mayer L., Governato F., 2015, *MNRAS*, **447**, 2123
- Colpi M., 2014, *Space Sci. Rev.*, **183**, 189
- Dabringhausen J., Hilker M., Kroupa P., 2008, *MNRAS*, **386**, 864
- Davis B. L., Graham A. W., Cameron E., 2019, *ApJ*, **873**, 85
- Dayal P., Rossi E. M., Shiralilou B., Piana O., Choudhury T. R., Volonteri M., 2018, preprint, ([arXiv:1810.11033](https://arxiv.org/abs/1810.11033))
- Dehnen W., 1993, *MNRAS*, **265**, 250
- Dotti M., Colpi M., Haardt F., Mayer L., 2007, *MNRAS*, **379**, 956
- Enoki M., Inoue K. T., Nagashima M., Sugiyama N., 2005, Annual Report of the National Astronomical Observatory of Japan, **7**, 34
- Fiacconi D., Mayer L., Roškar R., Colpi M., 2013, *ApJ*, **777**, L14
- Gebhardt K., et al., 1996, *AJ*, **112**, 105
- Geha M., et al., 2017, *ApJ*, **847**, 4
- Glass L., et al., 2011, *ApJ*, **726**, 31
- Goicovic F. G., Sesana A., Cuadra J., Stasyszyn F., 2017, *MNRAS*, **472**, 514
- Graham A. W., Scott N., 2015, *ApJ*, **798**, 54
- Graham A. W., Erwin P., Trujillo I., Asensio Ramos A., 2003, *AJ*, **125**, 2951
- Greene J. E., Ho L. C., Barth A. J., 2008, *ApJ*, **688**, 159
- Hernquist L., 1990, *ApJ*, **356**, 359
- Holley-Bockelmann K., Sigurdsson S., 2006, preprint, ([arXiv:astro-ph/0601520](https://arxiv.org/abs/astro-ph/0601520))
- Jaffe W., 1983, *MNRAS*, **202**, 995
- Khan F. M., Just A., Merritt D., 2011, *ApJ*, **732**, 89
- Khan F. M., Preto M., Berczik P., Berentzen I., Just A., Spurzem R., 2012a, *ApJ*, **749**, 147
- Khan F. M., Berentzen I., Berczik P., Just A., Mayer L., Nitadori K., Callegari S., 2012b, *ApJ*, **756**, 30
- Khan F. M., Holley-Bockelmann K., Berczik P., Just A., 2013, *ApJ*, **773**, 100
- Khan F. M., Fiacconi D., Mayer L., Berczik P., Just A., 2016, *ApJ*, **828**, 73
- Khan F. M., Berczik P., Just A., 2018a, *A&A*, **615**, A71
- Khan F. M., Capelo P. R., Mayer L., Berczik P., 2018b, *ApJ*, **868**, 97
- Klein A., et al., 2016, *Phys. Rev. D*, **93**, 024003
- Kormendy J., Ho L. C., 2013, *ARA&A*, **51**, 511
- Läscher R., Greene J. E., Seth A., van de Ven G., Braatz J. A., Henkel C., Lo K. Y., 2016, *ApJ*, **825**, 3
- Latif M. A., Ferrara A., 2016, *Publ. Astron. Soc. Australia*, **33**, e051
- Lodato G., Nayakshin S., King A. R., Pringle J. E., 2009, *MNRAS*, **398**, 1392
- Lupi A., Haardt F., Dotti M., Colpi M., 2015, *MNRAS*, **453**, 3437
- Márquez I., Lima Neto G. B., Capelato H., Durret F., Gerbal D., 2000, *A&A*, **353**, 873
- Mayer L., 2013, *Classical and Quantum Gravity*, **30**, 244008
- Mayer L., 2017, in *Journal of Physics Conference Series*. p. 012025 ([arXiv:1703.00661](https://arxiv.org/abs/1703.00661)), doi:10.1088/1742-6596/840/1/012025
- Mayer L., Kazantzidis S., Madau P., Colpi M., Quinn T., Wadsley J., 2007, *Science*, **316**, 1874
- Mayer L., Tamburello V., Lupi A., Keller B., Wadsley J., Madau P., 2016, *ApJ*, **830**, L13
- Merritt D., Poon M. Y., 2004, *ApJ*, **606**, 788
- Mezcua M., 2017, *International Journal of Modern Physics D*, **26**, 1730021
- Mezcua M., Civano F., Marchesi S., Suh H., Fabbiano G., Volonteri M., 2018, *MNRAS*, **478**, 2576
- Milosavljević M., Merritt D., 2003, in *Centrella J. M., ed., American Institute of Physics Conference Series Vol. 686, The Astrophysics of Gravitational Wave Sources*. pp 201–210 ([arXiv:astro-ph/0212270](https://arxiv.org/abs/astro-ph/0212270)), doi:10.1063/1.1629432
- Muñoz R. R., Côté P., Santana F. A., Geha M., Simon J. D., Oyarzún G. A., Stetson P. B., Djorgovski S. G., 2018, *ApJ*, **860**, 66
- Nguyen D. D., et al., 2018, *ApJ*, **858**, 118
- Peters P. C., Mathews J., 1963, *Physical Review*, **131**, 435
- Pfister H., Lupi A., Capelo P. R., Volonteri M., Bellovary J. M., Dotti M., 2017, *MNRAS*, **471**, 3646
- Pfister H., Volonteri M., Dubois Y., Dotti M., Colpi M., 2019, preprint, ([arXiv:1902.01297](https://arxiv.org/abs/1902.01297))
- Plowman J. E., Hellings R. W., Tsuruta S., 2011, *MNRAS*, **415**, 333
- Prugniel P., Simien F., 1997, *A&A*, **321**, 111
- Quinlan G. D., 1996, *New Astron.*, **1**, 35
- Read J. I., Goerdt T., Moore B., Pontzen A. P., Stadel J., Lake G., 2006, *MNRAS*, **373**, 1451
- Reines A. E., Volonteri M., 2015, *ApJ*, **813**, 82
- Reines A. E., Greene J. E., Geha M., 2013, *ApJ*, **775**, 116
- Rhook K. J., Wyithe J. S. B., 2005, *MNRAS*, **361**, 1145
- Ricarte A., Natarajan P., 2018, *MNRAS*, **474**, 1995
- Roškar R., Fiacconi D., Mayer L., Kazantzidis S., Quinn T. R., Wadsley J., 2015, *MNRAS*, **449**, 494
- Savorgnan G., Graham A. W., Marconi A., Sani E., Hunt L. K., Vika M., Driver S. P., 2013, *MNRAS*, **434**, 387
- Scott N., Graham A. W., Schombert J., 2013, *ApJ*, **768**, 76
- Sérsic J. L., 1963, *Boletín de la Asociación Argentina de Astronomía La Plata Argentina*, **6**, 41
- Sérsic J. L., 1968, *Atlas de Galaxias Australes*. Observatorio Astronómico
- Sesana A., Khan F. M., 2015, *MNRAS*, **454**, L66
- Sesana A., Haardt F., Madau P., 2006, *ApJ*, **651**, 392
- Sesana A., Gair J., Berti E., Volonteri M., 2011a, *Phys. Rev. D*, **83**, 044036
- Sesana A., Gualandris A., Dotti M., 2011b, *MNRAS*, **415**, L35
- Souza Lima R., Mayer L., Capelo P. R., Bellovary J. M., 2017, *ApJ*, **838**, 13
- Tamanini N., Caprini C., Barausse E., Sesana A., Klein A., Petiteau A., 2016, *J. Cosmology Astropart. Phys.*, **4**, 002
- Tamburello V., Capelo P. R., Mayer L., Bellovary J. M., Wadsley J. W., 2017, *MNRAS*, **464**, 2952
- Tamfal T., Capelo P. R., Kazantzidis S., Mayer L., Potter D., Stadel J., Widrow L. M., 2018, *ApJ*, **864**, L19
- Terzić B., Graham A. W., 2005, *MNRAS*, **362**, 197
- Tremaine S., Richstone D. O., Byun Y.-I., Dressler A., Faber S. M., Grillmair C., Kormendy J., Lauer T. R., 1994, *AJ*, **107**, 634
- Tremmel M., Karcher M., Governato F., Volonteri M., Quinn T. R., Pontzen A., Anderson L., Bellovary J., 2017, *MNRAS*, **470**, 1121
- Van Wassenhove S., Volonteri M., Walker M. G., Gair J. R., 2010, *MNRAS*, **408**, 1139
- Van Wassenhove S., Capelo P. R., Volonteri M., Dotti M., Bellovary J. M., Mayer L., Governato F., 2014, *MNRAS*, **439**, 474
- Vasiliev E., 2014, *Classical and Quantum Gravity*, **31**, 244002
- Vasiliev E., 2016, in *Meiron Y., Li S., Liu F.-K., Spurzem R., eds, IAU Symposium Vol. 312, Star Clusters and Black Holes in Galaxies across Cosmic Time*. pp 92–100 ([arXiv:1411.1762](https://arxiv.org/abs/1411.1762)), doi:10.1017/S1743921315007607
- Vasiliev E., Antonini F., Merritt D., 2015, *ApJ*, **810**, 49
- de Vaucouleurs G., 1948, *Annales d'Astrophysique*, **11**, 247
- de Vaucouleurs G., 1959, *Handbuch der Physik*, **53**, 275,311
- del Valle L., Escala A., Maureira-Fredes C., Molina J., Cuadra J., Amaro-Seoane P., 2015, *ApJ*, **811**, 59
- van der Wel A., et al., 2014, *ApJ*, **788**, 28

This paper has been typeset from a $\text{\TeX}/\text{\LaTeX}$ file prepared by the author.